Published in final edited form as:

Ultrason Imaging. 2016 September ; 38(5): 346–358. doi:10.1177/0161734615617940.

Experimental Validation of ARFI Surveillance of Subcutaneous Hemorrhage (ASSH) Using Calibrated Infusions in a Tissue-Mimicking Model and Dogs

Rebecca E. Geist[1], **Chase H. DuBois**[1,2], **Timothy C. Nichols**[3,4], **Melissa C. Caughey**[3], **Elizabeth P. Merricks**[4], **Robin Raymer**[4], and **Caterina M. Gallippi**[1]

[1]Joint Department of Biomedical Engineering, University of North Carolina at Chapel Hill, Chapel Hill, NC, USA and North Carolina State University, Raleigh, NC, USA

[2]Cortical Metrics, LLC, Chapel Hill, NC, USA and North Carolina State University, Raleigh, NC USA

[3]Department of Medicine, University of North Carolina at Chapel Hill, Chapel Hill, NC, USA

[4]Department of Pathology and Laboratory Medicine, University of North Carolina at Chapel Hill, Chapel Hill, NC, USA

Abstract

Acoustic radiation force impulse (ARFI) Surveillance of Subcutaneous Hemorrhage (ASSH) has been previously demonstrated to differentiate bleeding phenotype and responses to therapy in dogs and humans, but to date, the method has lacked experimental validation. This work explores experimental validation of ASSH in a poroelastic tissue-mimic and *in vivo* in dogs. The experimental design exploits calibrated flow rates and infusion durations of evaporated milk in tofu or heparinized autologous blood in dogs. The validation approach enables controlled comparisons of ASSH-derived bleeding rate (BR) and time to hemostasis (TTH) metrics. In tissue-mimicking experiments, halving the calibrated flow rate yielded ASSH-derived BRs that decreased by 44% to 48%. Furthermore, for calibrated flow durations of 5.0 minutes and 7.0 minutes, average ASSH-derived TTH was 5.2 minutes and 7.0 minutes, respectively, with ASSH predicting the correct TTH in 78% of trials. In dogs undergoing calibrated autologous blood infusion, ASSH measured a 3-minute increase in TTH, corresponding to the same increase in the calibrated flow duration. For a measured 5% decrease in autologous infusion flow rate, ASSH detected a 7% decrease in BR. These tissue-mimicking and *in vivo* preclinical experimental validation studies suggest the ASSH BR and TTH measures reflect bleeding dynamics.

Keywords

ASSH; ARFI; acoustic radiation force; hemorrhage; bleeding; hemostasis; dog; tofu; ultrasound

Corresponding Author: Caterina M. Gallippi, Ph.D., University of North Carolina at Chapel Hill, 150 MacNider Hall, CB 7575, Chapel Hill, NC 27599, USA., cmgallip@email.unc.edu.

Introduction

Prolonged or undetected bleeding can increase the risk of mortality and morbidity in patients with disordered bleeding, whether induced or inherited. Induced disordered bleeding often results from the introduction of anticoagulants prior to invasive surgical procedures[1,2]. After surgical procedures, clinically standard care may be blind to subcutaneous bleeding, despite available therapies if excessive bleeding is diagnosed[3,4]. Analysis of subcutaneous bleeding dynamics could lead to diagnoses that improve patient outcomes, but this analysis requires an *in vivo* subcutaneous bleeding detection method. Additionally, inherited disordered bleeding, as with hemophilia A or von Willebrand's disease, requires lifelong therapy and management[5]. Advances in treatment would benefit from the development of improved pharmacotherapies to control bleeding response. Accurately assessing bleeding response for the development of pharmacotherapies requires an analysis method that is *in vivo*, reproducible, and validated. Differentiating bleeding phenotype is an important tool in the development and testing of pharmacotherapies, and assessing the subcutaneous bleeding dynamics is diagnostically relevant, but there is currently no reproducible method to assess *in vivo* bleeding dynamics available.

Commonly used first-line clotting tests to evaluate bleeding risk in patients include activated partial thromboplastin time (APTT) and prothrombin time (PT). Both APTT and PT are *in vitro* measures that require the introduction of exogenous reagents, and thus do not accurately reflect *in vivo* bleeding response[1,6,7]. Alternatively, standardized skin bleeding time (BT) is an *in vivo* hemostasis test that can be performed, but this method suffers from a lack of reproducibility and heavy reliance on testing location[1,8,9,10]. Other tests have been developed to evaluate primary hemostasis, but these are not widely used or validated[1,11]. Currently, there is no reproducible method to assess *in vivo* bleeding dynamics available, which creates a need for an *in vivo* hemorrhage detection method.

A novel hemorrhage detection method, ARFI Surveillance of Subcutaneous Hemorrhage (ASSH), uses acoustic radiation force (ARF) impulses to induce displacement in soft tissue and conventional ultrasonic tracking pulses to monitor the displacement response. Tissue containing hemorrhage exhibits heightened displacement variance, which is evaluated as the variance of the second time-derivative of displacement following soft tissue recovery, as described in Scola et al[12]. Thus, placing an adaptive threshold on the variance identifies pixels corresponding to regions of hemorrhage, and the area of hemorrhage is measured through several serially-acquired imaging frames over time. Then, metrics describing bleeding dynamics, bleeding rate (BR) and time to hemostasis (TTH), are measured as the rate of change in the detected hemorrhagic area and the time at which the rate decreases to zero, respectively.

We have previously shown that ASSH-derived BR and TTH metrics differentiate bleeding phenotype in dogs with hemophilia A and von Willebrand disease in naive versus treated states and versus control dogs with no known bleeding disorders[12,13,14]. We have also demonstrated that ASSH distinguishes BR and TTH at femoral arteriotomy following diagnostic percutaneous coronary catheterization in humans treated with standard of care manual compression alone versus standard of care augmented by hemostatic dressing[15].

Although our previous body of work demonstrates that ASSH-derived BR and TTH measures are consistent with expected variation with phenotype and/or treatment, the lack of an alternative, validated method for direct measurement of subcutaneous bleeding dynamics has precluded *in vivo* ASSH validation. If not in the context of true *in vivo* bleeding, the purpose of this study is to experimentally validate ASSH BR and TTH measures using calibrated flow rates and durations in tissue-mimicking materials and in dogs, *in vivo*.

This work explores an experimental validation of this method, utilizing tofu as a tissue mimicking model and animal trials. In previous research, tofu has been examined as a poroelastic tissue mimic[16,17,18], with similar speed of sound and without the effect of experiencing any rigor expected with deceased animal tissue. Evaporated milk has been shown to have properties suited for use as a blood mimic, while avoiding the clotting properties of blood [19,20,21,22]. The animal trials, utilizing dogs with no known bleeding abnormalities, infused native blood from a femoral artery puncture into an avascular space. To slow clotting on artificial surfaces, the dogs were intravenously heparinized.

Method

Infusing Evaporated Milk into Tofu

Figure 1 demonstrates the experimental setup for infusing evaporated milk into tofu. For each trial, tofu (Vitasoy Firm) samples were weighed and placed in a water bath, in Figure 1D. Concurrently, evaporated milk (My Essentials) was mixed with food dye, Figure 1B. With B-mode ultrasound guidance (Figure 1A), a 20 gauge catheter sheath connected to the reservoir of dyed evaporated milk was inserted into the tofu at the approximate focus depth (2cm) and at the approximate lateral center of the 1.4cm imaging window. The imaging transducer was then displaced approximately 3 mm in elevation to avoid imaging interference from the catheter.

A peristaltic pump (Cole Parmer Masterflex L/S 7550-30 with Masterflex L/S Easy-Load II Head 77200-60, Figure 1C) was used to transfer the solution into tofu through a 20 gauge catheter sheath at controlled rates. Three combinations of programmed flow rates and durations were examined: 5.0 ml/min for 5.0 min, 2.5 ml/min for 5.0min, and 5.0 ml/min for 7.0 min. Each of the three combinations of programmed flow rates and duration underwent 6 repeated measures in separate trials, for 18 total experiments.

ARFI imaging was manually synchronized to the start of the flow pump, and an ARFI frame was acquired every minute for 12 minutes. For ARFI imaging, ARF impulses were centered at 4.21 MHz with an F/1.5 focal configuration and were 300 cycles (70 μs) in duration. Tracking pulses were centered at 6.15 MHz with an F/1.5 focal configuration and were 2 cycles in duration. ARFI beam sequences consisted of an ARF excitation preceded by at least two tracking lines for reference and followed by 58 tracking lines in the region of ARF excitation. This beam sequence was applied in 40 lateral positions spaced 0.35 mm apart, spanning a 1.4 cm lateral field of view, by alternating the region of excitation from the left to the right side of the image frame. Imaging was conducted using a Siemens Acuson Antares imaging system specially equipped for research purposes and a VF7-3 linear array (Siemens Medical Solutions USA Inc, Ultrasound Division).

Calibrated Autologous Infusion in Dogs

ASSH imaging was performed to monitor calibrated infusions of heparinized autologous blood in two dogs. (All animal trials received prior approval by the University of North Carolina at Chapel Hill Institutional Animal Care & Use Committee.)

Each dog was anesthetized. Typically, dogs are pre- medicated with atropine (0.022 – 0.044 mg/kg SQ, IM) and butorphanol (0.2 – 0.4 mg/kg IM, SQ, or IV) for sedation, and then anesthesia is induced with propofol ("Propoflo" per manufacturer label at 5.5 mg/kg IV or "Propoflo28" per manufacturer label at 7.6 mg/kg IV) over 60 to 90 seconds followed by immediate intubation and transition to isoflurane to effect (~2%). Anesthesia is evaluated by heart rate, respiratory rate, blood pressure, oxygen saturation, end-tidal CO^2, and persistence or absence of palpebral, corneal and withdrawal reflexes. In addition, body temperature is monitored and maintained with warming blankets as needed.

The dog was positioned in dorsal recumbancy. Overlying fur is shaved from each hind limb leg and the skin is cleaned in an aseptic fashion with alcohol and betadine. Heparin (35 units/kg) was administered intravenously to prevent clotting during infusion.

The experimental setup is depicted in a flow chart and diagram shown in Figure 2. Similarly, a picture of the experimental setup is shown in Figure 3. With B-Mode ultrasound guidance, the right femoral artery was cannulated with a 5F arterial sheath (Figure 2A, Figure 3A), and a stopcock was positioned at the catheter to selectively stop or allow blood flow out of the artery. A catheter was also inserted using B-Mode guidance into peri-femoral muscle in the left hind limb (Figure 2D, Figure 3D), with particular attention given to avoiding obvious vasculature in the region. The puncturing needle and catheter were filled with saline prior to insertion to prevent introducing air bubbles into the muscle tissue. The imaging transducer (Figure 2E, Figure 3E), held in position using a stereotactic clamp (Figure 2F, Figure 3E), was then displaced approximately 5 mm in elevation to avoid imaging interference from the catheter.

With both catheters in place, one in the right femoral and the other in peri-femoral muscle in the left hind leg, sterile tubing with non-hemolytic properties (MasterFlex PharMed BPT L/S #13, Figure 3C) was first filled with saline (to prevent the introduction of air bubbles into the closed system) and then connected to the stopcock. The tubing was fed through a computerized peristaltic flow pump (Masterflex L/S with Easy-Load II Head, Figure 3B), which controlled the flow rate and duration. The flow pump was programmed for a flow rate of 5.0 ml/min, but the actual flow rate was calibrated by pumping blood into a graduated cylinder for 1 min. Programmed flow rates of 5.0mL were found to not clot for 7–10 minute trials, but lower rates produced clots in tubing. We observed that the actual flow rates were higher than the programmed rates, which may be attributable to arterial pressure. After flow rate calibration, the open end of the tubing was connected to the catheter inserted in the peri-femoral muscle in the left hind limb. In this manner, when the stopcock was released and the flow pump enabled, heparinized autologous blood flowed from the femoral artery in the right hind limb into the peri-femoral muscle in the left hind limb via the peristalitic pump. Two durations were examined: 5.0 ml/min for 10.0min, and 5.0 ml/min for 7.0 min.

ARFI imaging was manually synchronized to the start of the flow pump, and an ARFI frame was acquired every minute for 20 minutes. ARFI imaging sequences were not altered from sequences used on tofu. Imaging was conducted using a Siemens Acuson Antares imaging system specially equipped for research purposes and a VF7-3 linear array (Siemens Medical Solutions USA Inc, Ultrasound Division).

Data Processing

Acquired raw radio frequency data were transferred to a separate workstation for post processing using custom ASSH software. The ASSH algorithm, as previously described by Scola et al [12], began by calculating ARFI-induced axial displacement profiles using 1-D normalized cross-correlation. Then, from these profiles, the variance of the second time derivative of displacement (acceleration) after time to soft tissue recovery (~ 4 ms) was calculated for each pixel experiencing peak displacement of at least 3 μm. The variance of acceleration (VoA) values were then organized into a histogram with finely sampled bins to identify the VoA peaks, which corresponded to VoAs achieved in tofu/soft tissue not containing hemorrhage. The upper bound on these peaks defined an initial lower VoA threshold for ASSH. Another local peak in the high VoA range of the histogram, associated with noise, was also identified to initialize an upper VoA threshold for ASSH.

With initial VoA thresholds selected, pixels with VoA values between the lower and upper VoA thresholds were considered to contain hemorrhage. Similarly, those pixels with VoA values outside the range of the lower and upper VoA thresholds was considered to not contain hemorrhage. In this manner, a binary image was created, encoding each pixel in the field of view as hemorrhage or not hemorrhage. Next, the initial VoA thresholds were iteratively updated using the constraint that the detected region of hemorrhage should be contiguous through space and time, and a final region of hemorrhage was detected using the updated VoA thresholds.

With region of hemorrhage identified, hemorrhagic area was calculated using the area ascribed to each pixel for each ARFI frame in the serial acquisitions. Then, rate of change in hemorrhagic area over time of serial acquisition was calculated using local (3 min sliding window) linear regression, and positive rate of change in hemorrhagic area was used as a metric for bleeding rate (BR). The time at which the BR stabilized to ≤ 0 mm^2/min for at least 5 min was considered the time to hemostasis onset (TTH).

ASSH BR and TTH were compared to the known flow rates of evaporated milk/blood and the known times at which the peristaltic pump was stopped.

Results

A representative ASSH imaging result in tofu is depicted in Figure 4. Panel (a) shows pixels identified as hemorrhagic (blue) superimposed on the corresponding B-Mode image. In panel (b), the identified hemorrhagic pixels are superimposed on a photograph of the tofu cross-section in the ASSH field of view. This tofu plane was matched to the ASSH imaging plane using fiducial markers, which are apparent in the B-Mode and tofu images (hyperechoic points numbered 1–7). For clarity, the tofu cross-section is shown without

ASSH hemorrhagic pixels superimposed to better depict the mimicked region of hemorrhage, indicated by the red dyed evaporated milk. Note that the axial range of ASSH imaging is limited to approximately 10 mm around the focus by the restriction that ASSH analysis be performed on pixels experiencing at least 3 microns of ARFI-induced peak displacement (see 'Data Processing' above).

Representative scatter plots of ASSH area of hemorrhage versus time for each of the three examined calibrated flow protocols are shown in Figure 5A. To facilitate visual comparisons, for each trial, the lowest detected hemorrhage area across all time was subtracted from the hemorrhagic area at each time point, such that each trial's minimum ASSH detected hemorrhage area was normalized to 0 mm^2. Importantly, this manner of normalization by subtraction did not impact the ASSH BR or TTH measurements. Note that for all three protocols, the ASSH area of hemorrhage increases over time to a peak hemorrhagic area and then decreases over time thereafter. This inflection point (circled) corresponds to the time at which the ASSH BR stabilizes to ≤ 0 mm^2/min, which is noted as the ASSH TTH (see 'Data Processing' in the Methods section above). Note that for protocols 1, 2, and 3 the ASSH-derived TTHs are respectively 5, 5, and 7 min, consistent with the programmed flow durations.

In addition to TTH, the ASSH hemorrhagic area versus time curves shown in 5(a) encode, as the positive rate of change in hemorrhagic area over time, the ASSH BR metric. Note that protocols 1 and 3, with matched infusion rates of 5.0 ml/min, exhibit similar positive rates of change in the ASSH detected hemorrhagic area. On the contrary, protocol 2, with an infusion rate half that of protocols 1 and 3, exhibits a slower positive change in ASSH hemorrhagic area over time. A final observation from Figure 5(a) is that the ASSH-derived area of hemorrhage decreased after the infusion stop, which we attribute to diffusion of evaporated milk into the surrounding tofu media. We note that such milk diffusion after infusion stop may have resulted in the larger dyed area in Figure 4C.

The box plots shown in figure 5(b) further represent all ASSH BR values measured in the calibrated tofu experiments for the three protocols. The mean BRs are approximately 3.1 mm^2/min, 1.6 mm^2/min, and 2.9 mm^2/min, for protocols 1, 2, and 3, respectively. In these tissue-mimicking experiments, halving the calibrated flow rate yielded ASSH-detected BRs that decreased by 44–48%. Statistical significance was found between the ASSH-derived BR between Protocol 1 and Protocol 2 (Wilcoxon Ranksum, α<0.01) and between Protocol 2 and Protocol 3 (Wilcoxon Ranksum, α<0.01). No statistically significant difference was found between ASSH BRs for protocols 1 and 3, which had matched infusion rates.

Figure 5(c) depicts all ASSH TTH measures for the three calibrated flow protocols against the known infusion time. For protocols 1 and 2, ASSH TTH matched the infusion duration in four out of six trials and was within ±1 minute of the true infusion duration in 2 out of six trials. For protocol 3, ASSH TTH matched the experimental infusion duration in six out of six trials. Overall, ASSH-detected TTH and known infusion time matched in 78% of all trials, while the remaining trials had ±1 minute error from the known infusion time. We note that with a temporal sampling period of 1 minute, a ±1 minute error is a single time sample offset from the true infusion stop. We attribute this ASSH TTH error, at least in part, to

manually synchronizing imaging and peristaltic pump starts. The average ASSH-detected TTH was 5.2 min and 7.0 min for trials with known infusion times of 5.0 min and 7.0 min, respectively.

Figure 6 depicts ASSH-detected hemorrhagic area versus time scatter plots for the two heparinized autologous blood infusion trials in dogs, *in vivo*. For each trial, the lowest detected hemorrhagic area was normalized by subtraction, as described above, to facilitate visual comparisons. ASSH area of hemorrhage increases initially to a peak value and then decreases. The peak (circled) corresponds to the time at which the ASSH-derived BR stabilizes to ≤ 0 mm^2/min, which is the ASSH TTH. For these two *in vivo* dog trials, ASSH-derived TTH was measured as 11 and 8 min, while the infusion stop time was 10 and 7 min, respectively. As was described above, we attribute this one-minute error in the TTH measurement to manual synchronization error. Note that the ASSH temporal sampling period was 1 min. Further, we attribute the decrease in ASSH hemorrhagic are after the infusion stop to diffusion of blood away from the ASSH imaging plane. In addition to TTH, the ASSH hemorrhagic area versus time graphs encode the ASSH BR, which was measured as 4.0 mm^2/min for trial 1 and 3.7 mm^2/min for trial 2. Table 1 summarizes the results of the autologous blood infusion trials. For the 5% decrease in the measured blood infusion rate between Trial 1 and Trial 2, the ASSH-detected BR decreased by 7%. Additionally, the 3 min difference in blood infusion durations between trials was exactly measured by ASSH TTH.

Discussion

The data presented in this study demonstrate the feasibility of using ASSH as a non-invasive *in vivo* method to describe bleeding dynamics.

In the first part of this work, tofu was used as a porous tissue-mimicking material and infused with evaporated milk as a blood mimic. In Figure 4, the area of red-dyed milk in the tofu cross-section is larger than detected area of hemorrhage in the corresponding ASSH imaging plane, which could be related to three factors. First, the VoA thresholds used for ASSH hemorrhage detection may have been set such that ASSH missed hemorrhagic pixels with low VoA, which would be expected in regions with lower ARFI displacement further from the ARFI focal depth. Second, the ASSH field of view is axially constrained to the region in which ARFI-induced displacements are ≥ 3 μm. Therefore, mimicked hemorrhage located outside of this region (approximately 10 mm around the axial focal depth) is not interrogated by ASSH. Third, milk diffusion may have resulted in an expanded dyed region at the time the tofu was sectioned (approximately 10 minutes after the time of the corresponding ASSH image).

For the calibrated tofu and milk studies, halving infusion rate resulted in a 44–48% decrease in ASSH-detected BR, which is significant at the $\alpha<0.01$ level (Wilcoxon Ranksum). This indicates that the ASSH BR metric is sensitive to reduction in infusion rate in this medium. Additionally, the TTH metric was examined in relation to the known infusion time. The ASSH-detected TTH matched the known infusion time in 78% of trials, with remaining trials having ±1 minute, or one temporal sampling unit, of error. This discrepancy may be

the result of synchronization error, as the starts of the flow pump and ASSH data acquisitions were manually synchronized.

Notably, tofu within a water bath is not susceptible to the same geometric constraints as *in vivo* tissue, which allowed the evaporated milk to slowly leak into the surrounding water bath. This slow leakage may have resulted in a lower than expected concentration of blood mimic within the imaging region. Additionally, evaporated milk does not clot. This experiment benefits from lack of clotting through consistent flow throughout infusion duration, but clotting is a critical factor in true bleeding dynamics *in vivo*. A non-clotting blood mimic was selected in this validation experimental setup specifically to allow a constant infusion rate.

In the second part of this work, native heparinized blood was infused *in vivo* into a peri-femoral avascular space in an anesthetized dog. Two trials were performed at similar infusion rates, with a three-minute difference in infusion times. Although the infusion rates were similar, ASSH-detected BR reflected the small difference in infusion rates. This could indicate that the ASSH BR metric is sensitive to even small differences in infusion rate, but more investigation is needed to calibrate the degree of error in ASSH BR measures. The three-minute difference in infusion time was reflected in the ASSH-detected TTH metrics. For both dog trials, TTH was overestimated by approximately one minute. As described above, this error may be related to manually synchronizing the starts of the flow pump and ASSH data acquisitions.

It is important to consider that in both tofu and dog studies, the ASSH-detected region of hemorrhage was observed to decrease after the infusion stop time. We attribute this decrease to diffusion of milk/blood away from the ASSH imaging plane. Such diffusion has the potential to impact ASSH performance. If the rate of diffusion out of the ASSH imaging plane exceeds the rate of bleeding into the ASSH imaging plane, such that the overall ASSH hemorrhagic area decreases over time despite on-going bleeding, ASSH will falsely detect hemostasis. Moreover, for rates of diffusion away from the ASSH imaging plane that are less than but comparable to the rate of bleeding into the ASSH imaging plane, ASSH-derived BR will be underestimated. The experiments conducted herein involved infusion rates (2.5 – 5.6 ml/min) that were two orders of magnitude smaller than the volume flow rate of blood in the human femoral artery (350 ml/min)[28] Even for these very slow infusion rates, the diffusion of milk/blood away from the ASSH imaging plane did not inhibit ASSH from appropriately estimating TTH (within ± the one-minute temporal sampling unit) or relative differences in BR. Therefore, it is expected that ASSH will be clinically relevant for monitoring hemostasis at femoral artery punctures, such as those experienced with percutaneous coronary catheterization. However, ASSH's application to monitoring substantially lower rates of hemorrhage, for example from much smaller vessels, may be challenged by diffusion rate.

The most notable limitation of this body of work is the small number of experiments. Despite the small number, significant differences were seen in the tissue mimicking experiments, with promising in vivo results. Another potential shortcoming was the limited axial ASSH range (approximately 10 mm surrounding the focal depth), which was imposed

by requiring that the detected ARF-induced peak displacement be ≥ 3 microns. Future work will expand ASSH's axial range. Finally, ASSH BR was estimated using local (3-minute sliding window) linear regression applied to the derived ASSH hemorrhagic area versus time curves, but a nonlinear polynomial regression may achieve superior performance. This will be a topic of future investigation. Overall, this work demonstrates the feasibility of ASSH BR and TTH metrics for detecting changes in calibrated infusion rates and infusion times in a tissue mimicking model and in dogs, in vivo.

Conclusion

This pilot work demonstrates that changes in calibrated infusion rates and durations are reflected in ASSH-derived BR and TTH metrics. In a tofu and evaporated milk hemorrhage mimicking model, halving the infusion rate resulted in a 44–48% reduction in ASSH-detected BR (Wilcoxon Ranksum, α<0.01), and ASSH correctly assigned TTH in 78% of trials. In an *in vivo* dog model of hemorrhage, a 5% reduction in flow rate was reflected in 7% decrease in ASSH-detected BR, and a three-minute increase in flow duration was accurately measured by ASSH TTH. In all tissue-mimicking and dog trials in these studies, ASSH detected TTH was within 1 minute, corresponding to 1 time sampling interval, of the known infusion time. These data suggest that ASSH-derived BR and TTH metrics characterize hemorrhage dynamics.

References

1. Chee YL, Crawford JCC, Watson HG, Greaves M. Guidelines on the assessment of bleeding risk prior to surgery or invasive procedures. British J of Haemotology. 2008; 140:496–504.
2. Chhatriwalla AK, Amin AP, Kennedy KF, House JA, Cohen DJ, Rao SV, Messenger JC, Marso SP. Association between bleeding events and in-hospital mortality after percutaneous coronary intervention. J of the American Med Assoc. 2013; 309(10):1022–29.
3. Bangalore S, Bhatt DL. Femoral Artery Access and Closure. Diagnostic and Therapeutic Cardiovascular Procedures. 2011; 124:147–56.
4. Merriweather N, Sulzbach-Hoke LM. Managing Risk of Complications at Femoral Vascular Access Sites in Percutaneous Coronary Intervention. Critical Care Nurse. 2012; 32(5):16–29.
5. Mejia-Carvajal C, Czapek EE, Valentino LA. Life expectancy in hemophilia outcome. J of Thrombosis and Haemostasis. 2006; 4:507–9.
6. Fowler A, Perry DJ. Laboratory monitoring of haemostasis. Anesthesia. 2015; 70:68–72.
7. Fukuda T, Honda Y, Kamisato C, Morishima Y, Shibano T. Reversal of anticoagulant effects of edoxaban, an oral, direct factor Xa inhibitor, with haemostatic agents. Blood Coagulation, Fibrinolysis, and Cellular Haemostasis. 2012; 107(2):253–9.
8. Mezzano D, Quiroga T, Periera J. The Level of Laboratory Testing Required for Diagnosis or Exclusion of a Platelet Function Disorder Using Platelet Aggregation and Secretion Assays. 2009; 35(2):242–54.
9. Paniccia R, Priora R, Liotta AA, Maggini N, Abbate R. Assessment of platelet function: Laboratory and point-of-care methods. World J of Translational Medicine. 2014; 3(3):69–83.
10. Podda GM, Bucciarelli P, Lussana F, Lecchi A, Cattaneo M. Usefulness of PFA-100 testing in the diagnostic screening of patients with suspected abnormalities of hemostasis: comparison with the bleeding time. J of Thrombosis and Haemostasis. 2007; 5:2393–8.
11. Ganter, MT., Hofer, CK. Point-of-Care Coagulation Monitoring. In: Ehrenfeld, JM., Cannesson, M., editors. Monitoring Technologies in Acute Care Environments. New York, USA: Springer; 2014. p. 329-42.

12. Scola MR, Nichols TC, Zhu H, Caughey MC, Merricks EP, Raymer RA, Margaritis P, High KA, Gallippi CM. ARFI ultrasound monitoring of hemorrhage and hemostasis *in vivo* in canine von Willebrand disease and hemophilia. Ultrasound Med Biol. 2011; 37(12):2126–32. [PubMed: 22033127]
13. Scola MR, Baggesen LM, Nichols TC, Key NS, Gallippi CM. A review of current methods for assessing hemostasis *in vivo* and introduction to a potential alternative approach. Thrombosis Research. 2012; 129(2):S57–61. [PubMed: 22405050]
14. Geist RE, Nichols TC, Merricks EP, Caughey MC, Gallippi CM. *In Vivo* ARFI Surveillance of Subcutaneous Hemorrhage (ASSH) for Monitoring rcFVIII Dose Response in Hemophilia A Dogs. IEEE IUS Proceedings. 2014:2296–2299.
15. Behler RH, Scola MR, Nichols TC, Caughey MC, Fisher MW, Zhu H, Gallippi CM. ARFI Ultrasound for *In Vivo* Hemostasis Assessment Postcardiac Catheterization, Part II: Pilot Clinical Results. Ultrasonic Imaging. 2009; 31(3):159–71. [PubMed: 19771959]
16. Wu J. Tofu as a Tissue-Mimicking material. Ultrasound Med Biol. 2001; 27(9):1297–300. [PubMed: 11597372]
17. Culjat MO, Goldenberg D, Tewari P, Singh RS. A Review of Tissue Substitutes for Ultrasound Imaging. Ultrasound Med Biol. 2010; 36(6):861–73. [PubMed: 20510184]
18. Kim YT, Kim HC, Inada-Kim M, Jung SS, Yun YH, Jho MJ, Sandstrom K. Evaluation of Tissue Mimicking Quality of Tofu for Biomedical Ultrasound. Ultrasound Med Biol. 2009; 35(3):472–81. [PubMed: 19101073]
19. Culjat MO, Goldenberg D, Tewari P, Singh RS. A review of tissue substitutes for ultrasound imaging. Ultrasound Med Biol. 2010; 36(6):861–873. [PubMed: 20510184]
20. Madsen EL, Frank GR, Dong F. Liquid or Solid Ultrasonically Tissue-Mimicking Materials with very low scatter. Ultrasound Med Biol. 1998; 24(4):535–42. [PubMed: 9651963]
21. McDonald M, Lochhead S, Chopra R, Bronskill MJ. Multi-modality tissue-mimicking phantom for thermal therapy. Phys Med Biol. 2004; 49(13):2767–2778. [PubMed: 15285246]
22. Webb BH, Deysher EF, Potter FE. Effects of Storage Temperature on Properties of Evaporated Milk. J Dairy Sci. 1951; 34(11):1111–1118.
23. Miller AB, Hoogstraten B, Staquet M, Winkler A. Reporting results of cancer treatment. Cancer. 1981; 47(1):207–214. [PubMed: 7459811]
24. Webert KE, Arnold DM, Lui Y, Carruthers J, Arnold E, Heddle NM. A new tool to assess bleeding severity in patients with chemotherapy-induced thrombocytopenia. Transfusion. 2012; 52:2466–2474. [PubMed: 22486274]
25. Guyton, AC., Hall, JE. Textbook of Medical Physiology. 11. China: Saunders Elsevier; 2006. Overview of the Circulation; Medical Physics of Pressure, Flow, and Resistance; p. 161-170.
26. Klabunde, RE. Cardiovascular physiology concepts. Phyladelphia, PA: Lippincott, Williams, and Wilkins; 2005. p. 91-94.
27. Pinter SZ, Lacefield JC. Detectability of small blood vessels with high-frequency power doppler and selection and selection of wall filter cut-off belocity for microvascular imaging. Ultrasound Med Biol. 2009; 35(7):1217–1228. [PubMed: 19394752]
28. Lewis P, Psaila JV, Davies WT, McCarty K, Woodcock JP. Measurement of volume flow in the human common femoral artery using a duplex ultrasound system. Ultrasound Med Biol. 1986; 12(10):777–784. DOI: 10.1016/0301-5629(86)90075-X [PubMed: 2948313]

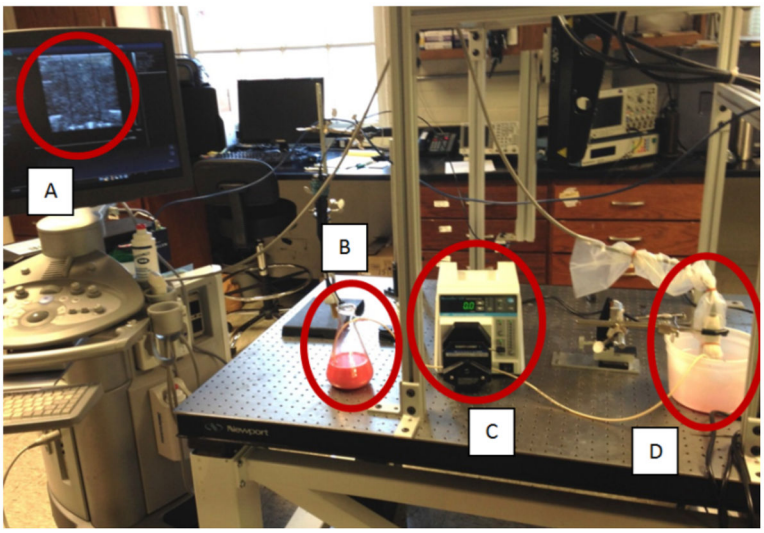

Figure 1.

A. Bmode image of lateral and elevational fiducial markers in tofu **B.** Evaporated milk and red food dye is drawn through L/S #13 tubing driven by **C.** the Masterflex L/S Peristaltic pump with easy-load head. **D.** L/S #13 tubing connects to the 18F sheath inserted into tofu for infusion, imaged by the VF7-3. transducer.

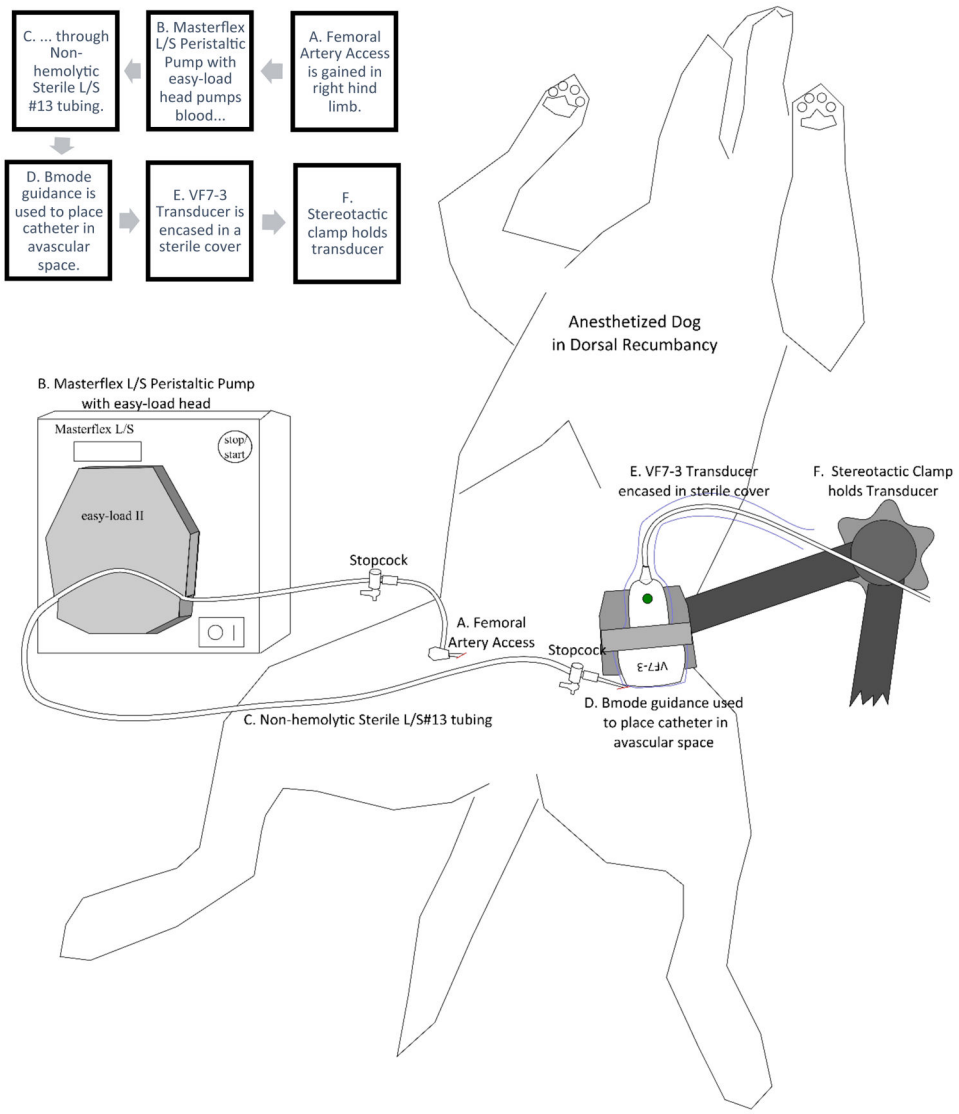

Figure 2.

Flow chart and diagram of experimental setup. Once the dog is anesthetized, heparinized, and in dorsal recumbancy, (A) femoral artery access is gained in the right hind limb. (B) The Masterflex L/S Peristaltic pump with easy-load head pumps native arterial blood through (C) Non-hemolytic sterile L/S #13 tubing. (D) A VF7-3 transducer provides Bmode guidance used to place the 5F catheter sheath into avascular space in the left hind limb prior to ASSH data acquisitions. The same transducer is then used for ASSH imaging. (E) The transducer is encased in a sterile cover, and (F) a stereotactic clamp holds the encased transducer.

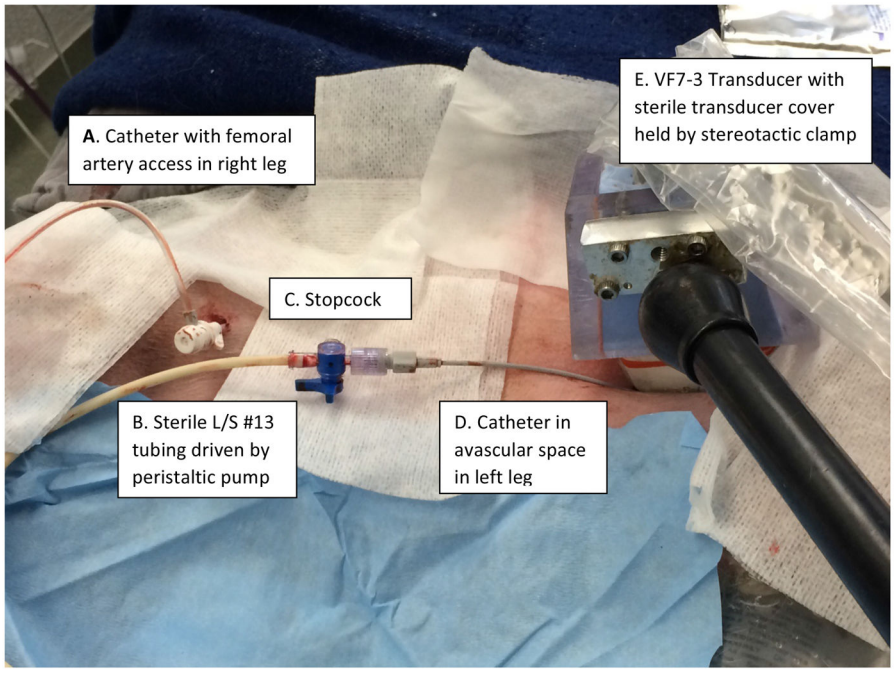

Figure 3.

Picture of experimental setup of dog in dorsal recumbancy shows (a) catheter with femoral artery access in right hind limb connected to (b) sterile L/S #13 tubing, driven by the peristaltic pump. The tubing is connected by (c) the stopcock to (d) the catheter in an avascular space in the left hind limb. This avascular space is imaged with (e) a VF7-3 transducer with sterile transducer cover held by a stereotactic clamp.

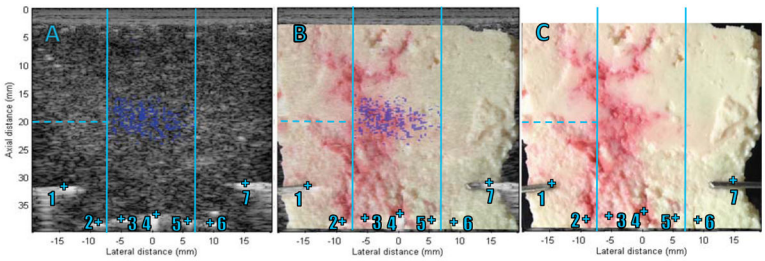

Figure 4.

(a) ASSH-detected binary image(blue) at infusion stop time overlaid on associated Bmode with fiducial markers 1–7 (b) Aligned ASSH and Bmode with gross tofu photo, including fiducial markers 1–7 (c) tofu photo with fiducial markers 1–7. In images a–c, lateral ASSH field of view is indicated with solid vertical lines, and axial ARF focus is indicated with dashed horizontal lines.

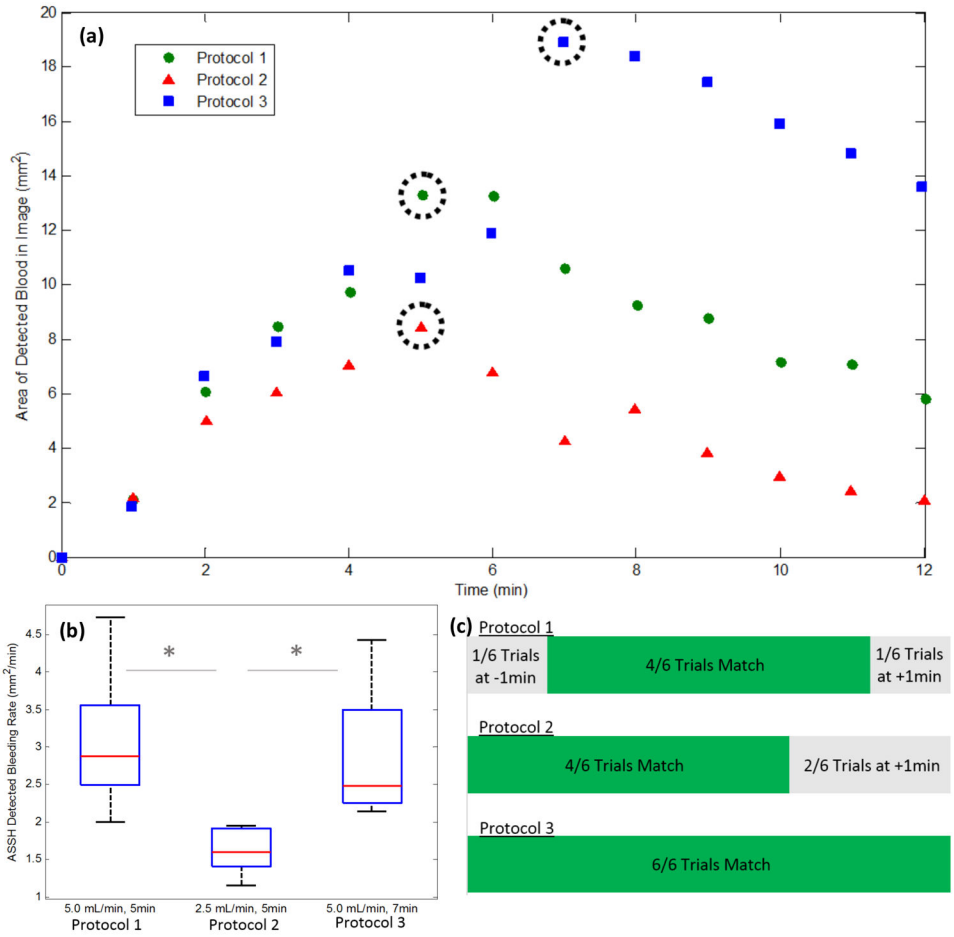

Figure 5.

(a) A representative example of ASSH-detected hemorrhage area versus time in tofu for each of Protocol 1 (5mL/min for 5.0min- green circle), Protocol 2 (2.5mL/min for 5.0 min- red triangle) and Protocol 3 (5mL/min for 7.0 min- blue square). For each example trial, ASSH hemorrhagic areas at the measured TTH are indicated with a dashed circle. Lowest detected area was normalized by subtraction to 0 mm^2 for the 3 examples. (b) Box plots of mean positive ASSH BR before TTH, showing median (red line), 25^{th} and 75^{th} percentiles (blue box), and the range of observed values (black dashed lines) for each of three protocols. Statistical significance ($\alpha<0.01$, Wilcoxon Ranksum, gray asterick) is indicated between Protocols 1 and 2, and between Protocols 2 and 3. (c) ASSH TTH detection for each of the three protocols. ASSH-detected TTH matched the calibrated flow duration (green) in 14/18 total trials, and is off by the sampling period of 1 minute (gray) in the remaining 4/18 trials.

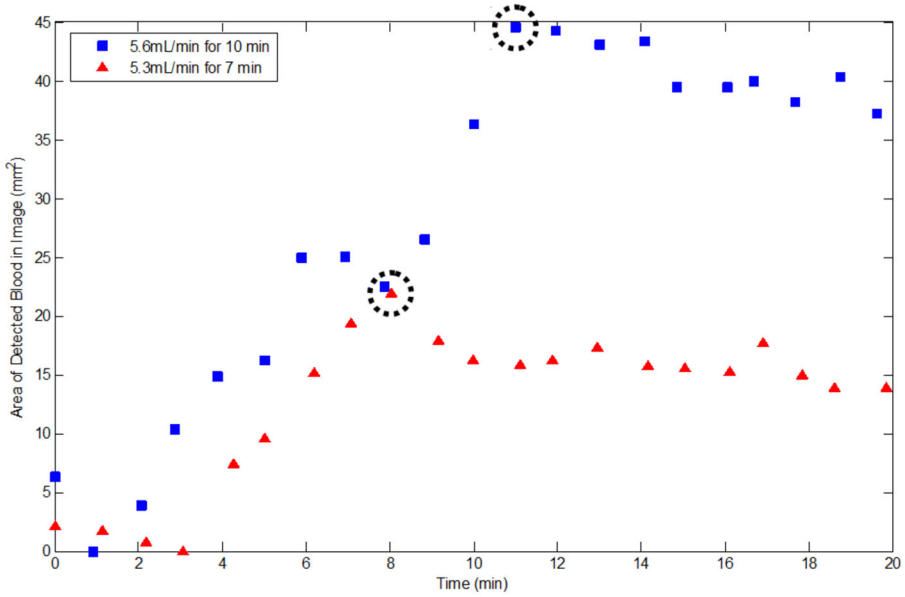

Figure 6.

ASSH-detected hemorrhagic area versus time for heparinized autologous blood infusion trials in dogs. Blood was infused into periarterial tissue at 5.6mL/min for 10 min (trial 1, blue squares) or 5.3mL/min for 7min (trial 2, red triangles). For both trials, the hemorrhagic area corresponding to the ASSH-derived TTH is circled. ASSH TTHs were 11 and 8 min for trials 1 and 2, respectively. Lowest detected area was normalized by subtraction to 0 mm^2 to facilitate visual comparisons.

Table 1

Heparinized Autologous Infusion

	Flow Rate	**Flow Time**	**ASSH BR**	**ASSH TTH**
Trial 1	5.6 mL/min	10.0 min	4.0 mm^2/min	11.0 min
Trial 2	5.3 mL/min	7.0 min	3.7 mm^2/min	8.0 min